参赛学生姓名：顾凌菲

中学：上海中学国际部

省份：上海

国家/地区：中国

指导老师 1 姓名：廖辉

指导老师 1 单位：上海中学国际部

指导老师 2 姓名：高峰青

指导老师 2 单位：苏州大学血液和血管疾病诊疗药物技术工程研究中心

论文题目：A Three-Layer Gradient PLGA/Hydroxyapatite Scaffold with pH-Responsive Curcumin Release for Combined Macrophage Immunomodulation and Osteogenic Induction

2026 S.T.Yau High School Science Award
仅用于2026丘成桐中学科学奖论文公示

A Three-Layer Gradient PLGA/Hydroxyapatite Scaffold with pH-Responsive Curcumin Release for Combined Macrophage Immunomodulation and Osteogenic Induction

Angelina Ling Fei Gu

Abstract

Bone repair after complex fractures remains an enduring clinical challenge. Conventional homogeneous biodegradable scaffolds are limited by uniform pore structure, mismatched degradation kinetics, limited immunomodulatory capacity, and insufficient osteogenic induction, which hinder their performance for complex bone repair. This study developed a novel three-layer gradient PLGA/HA scaffold loaded with curcumin to overcome these limitations. Distinct PLGA ratios and gradient HA and curcumin contents were designed for outer, middle and inner layers. Physicochemical characterizations showed that this gradient scaffold had more open, irregular porous structure with higher porosity compared with homogeneous scaffold, which underpinned its superior osteogenic performance, as evidenced by the significantly increased expression of osteogenic markers RUNX2 and ALP at both protein and mRNA levels. Benefiting from varied PLGA ratio across layers, the three-layer gradient scaffold realized a tunable degradation rate. It also achieved pH-responsive curcumin release: fast drug release under inflammatory pH 5.5 condition, while reduced drug leakage at physiological pH 7.4 condition. Moreover, curcumin released from the scaffold markedly suppressed pro-inflammatory M1 macrophage polarization, promoted reparative M2 macrophage polarization, and elevated anti-inflammatory IL-10 secretion. Collectively, this three-layer gradient scaffold with pH-responsive curcumin release exhibited favorable structural and degradative features, effective immunomodulatory function, and enhanced osteogenic capacity, representing a promising candidate biomaterial for complex bone repair and deserving further in-vivo validation toward clinical application.

Keywords: Bone repair; three-layer gradient scaffold; PLGA; HA; curcumin

2026 S.T. Yau High School Science Award
仅用于2026丘成桐中学科学奖论文公示

Contents

1 Introduction ····· 1

1.1 Background ····· 1
1.2 Objective and Innovation ····· 2
1.3 Research Question and Hypotheses ····· 3
1.4 Overall Study Design and Technical Roadmap ····· 3

2 Materials and Methodology ····· 4

2.1 Materials ····· 4
2.1.1 Chemicals ····· 4
2.1.2 Cells and Reagents ····· 5
2.1.3 Equipment ····· 5
2.2 Experimental Methods ····· 6
2.2.1 Fabrication of Scaffolds ····· 6
2.2.2 Scaffold Material Characterization ····· 7
2.2.3 Degradation Performance ····· 8
2.2.4 pH-Responsive Curcumin Release Test ····· 8
2.2.5 Evaluation of Anti-inflammatory Effects ····· 8
2.2.6 Evaluation of Osteogenic Differentiation Performance ····· 10

3 Results and Discussion ····· 11

3.1 Scaffold Morphology and Structure ····· 11
3.2 Porosity ····· 11
3.3 Chemical Structure (FT-IR Spectra) ····· 12
3.4 Crystalline Structure ····· 13
3.5 Degradation Behavior ····· 14
3.6 pH-responsive Drug Curcumin Profile ····· 15
3.7 Anti-inflammatory Effect ····· 16
3.8 Osteogenic Differentiation ····· 19

4 Future Plan ····· 21

5 Conclusion ····· 21

References ····· 23

Acknowledgements ····· 26

2026 S·T·Yau High School Science Award
仅用于2026丘成桐中学科学奖论文公示

1 Introduction

1.1 Background

Bone fractures are one of the most common and painful traumatic injuries worldwide, affecting millions of individuals and causing long-term physical disability across global populations [1]. A fractured bone requires a long recovery period and brings continuous physical discomfort and impaired mobility throughout the healing process. Approximately 5–10% of fracture patients develop bone nonunion and eventually require revision surgery [2]. Therefore, developing advanced biomaterials that can support efficient bone regeneration and improve postoperative healing microenvironments remains highly necessary.

Traditional permanent metallic implants have been widely used for fracture fixation, but they possess two prominent clinical drawbacks: first, a second surgery is mandatory for implant removal after bone healing, adding extra surgical trauma, pain and excessive medical expenditure for patients; second, the traditional permanent metallic implants possess no therapeutic function to suppress the sustained inflammation response induced by bone fracture, and such persistent inflammation state disrupts the bone microenvironment, inhibits osteoblast growth, delays tissue repair and causes continuous swelling and pain [3].

With the rapid development of tissue engineering, biodegradable polymer scaffolds have emerged as a promising alternative to permanent metallic implants to resolve the critical drawback of mandatory secondary surgery [4]. A large number of animal studies have confirmed that polymer scaffolds can support cell growth and promote skeletal tissue regeneration [5]. These temporary porous biomaterials degrade gradually inside the human body without the need of additional surgical extraction after bone repair, significantly reducing surgical trauma, pain, and clinical expenditure for fracture patients.

Nevertheless, conventional homogeneous biodegradable scaffolds still possess prominent limitations. They lack intrinsic therapeutic capacity for anti-inflammatory and immunomodulatory effects and osteogenic induction. On the other hand, most current scaffolds adopt simple, uniform structures with fixed degradation rates. These non-gradient structures cannot adapt to the dynamic biological demands across different bone-healing stages, leading

2026 Siyau High School Science Award
仅用于2026年成利中学科学奖论文公示

to obvious structural and functional defects that restrict their repair performance in clinic fracture treatments [6]. These practical limitations are well demonstrated in multiple animal studies focusing on polymer-based scaffold regeneration. Polo-Corrales (2014) investigated diverse bone graft techniques for skeletal fracture repair and bone defect regeneration. Although conventional grafting modalities achieved promising reparative outcomes, autografts incur donor site morbidity while allografts carry infection and immune rejection risks. Current substitutes still fail to fabricate living constructs comparable to native bone in structural and functional properties [7]. Zadpoor (2015) highlighted that geometrical parameters such as surface curvature, pore size and pore shape directly regulate cellular response and bone regeneration rate within porous scaffolds, yet few existing additively manufactured scaffolds harness geometric gradient architectures to optimize bone repair [8]. Even structurally customized PLA/PGA scaffolds designed for TMJ cartilage repair exhibits native-like mechanical strength; however, their single-layered structure fails to recapitulate the natural bone-cartilage transitional tissues [9]. Consequently, these homogeneous polymer scaffolds are only applicable to simple single-tissue repair and remain inadequate for treating complex bone fractures that require staged degradation, immunomodulation, and osteogenic induction.

1.2 Objective and Innovation

To address the above-mentioned drawbacks including mismatched degradation behavior, persistent postoperative inflammation, and insufficient osteogenic induction capacity, this study proposes a novel three-layer gradient Poly (lactic-co-glycolic acid) (PLGA) / hydroxyapatite (HA) scaffold loaded with curcumin. PLGA, HA and curcumin are promising biomaterials in bone fracture repair. PLGA enables control of degradation behavior through adjusting its lactic/glycolic monomer ratio (e.g. 50:50 PLGA degrades within 1–2 months, while 85:15 PLGA remains structurally stable for 6–12 months, matching the full timeline of bone healing) [10]. As the main inorganic component of natural bone, HA supports cell attachment and activates osteogenic signaling through the release of calcium and phosphate ions, effectively promoting bone reconstruction [11]. Curcumin is a natural anti-inflammatory compound, capable of regulating macrophage polarization and modulating the local immune

2026 S.-T. Yau High School Science Award
仅用于2026丘成桐中学科学奖公示

microenvironment, and when integrated into the scaffold, it can be released in a pH-responsive manner to alleviate postoperative inflammation [12].

Collectively, this study targets to fabricate a curcumin-loaded three-layer gradient scaffold, which integrates multiple functions: staged degradation, pH-responsive drug release, anti-inflammatory immunomodulatory therapy, and enhanced osteogenic induction, aiming to overcome the deficiencies of conventional homogeneous scaffolds.

1.3 Research Question and Hypotheses

The core research question of this study is: Can a curcumin-loaded three-layer gradient PLGA/HA scaffold achieve staged degradation, pH-responsive sustained curcumin release, effective inflammation suppression, and favorable osteogenic induction?

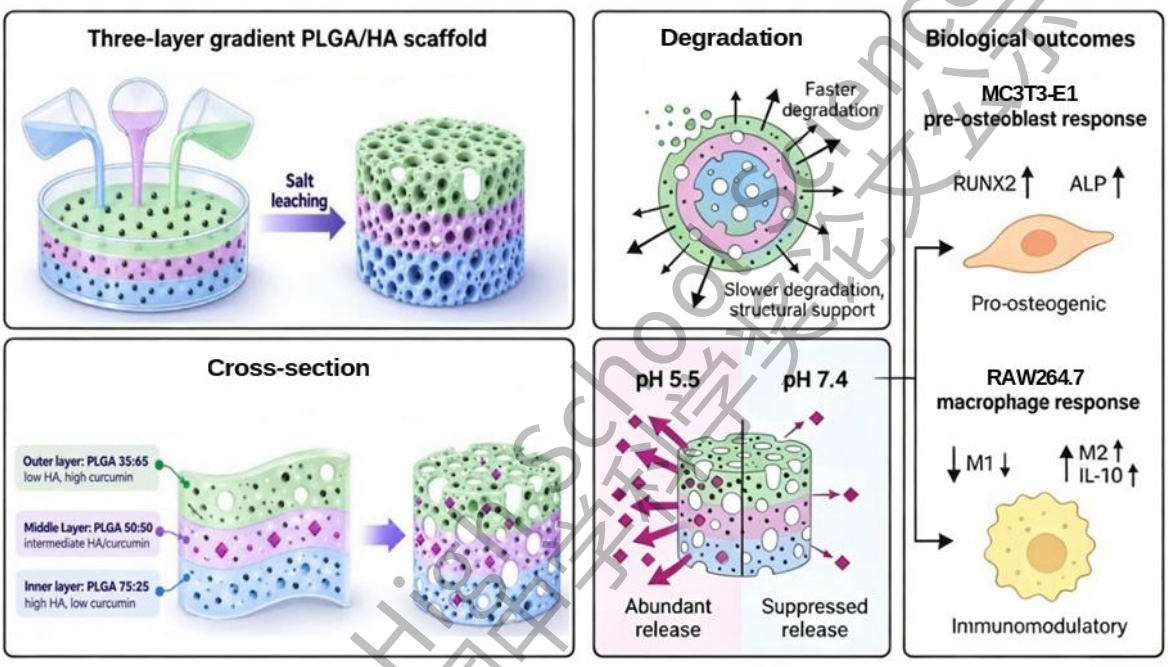
To answer the research question, three hypotheses are proposed. First, the three-layer gradient PLGA/HA scaffold will exhibit tunable staged degradation behavior compatible with the physiological bone healing cascade. Second, the curcumin-loaded three-layer gradient scaffold can realize pH-responsive curcumin release, suppress pro-inflammatory M1 macrophage polarization, promote anti-inflammatory M2 macrophage polarization, and boost the secretion of anti-inflammatory cytokine IL-10. Third, compared to homogeneous scaffolds, the three-layer gradient scaffold will more efficiently promote osteogenic differentiation of pre osteoblasts by upregulating the expression of core osteogenic markers RUNX2 and ALP.

1.4 Overall Study Design and Technical Roadmap

Herein, to address the limitations of conventional homogeneous biodegradable scaffolds and to test the above hypotheses, this study designs and fabricates a curcumin-loaded three-layer gradient PLGA/HA scaffold with layer-specific PLGA ratios (outer layer 35:65, middle layer 50:50, inner layer 75:25), gradient HA content, and gradient curcumin loading (**Scheme 1**). The scaffolds are prepared by sequential solvent casting and salt leaching, while homogeneous 50:50 PLGA/HA/curcumin scaffolds are fabricated as the control. The study then systematically evaluates the scaffold from material, drug-release, and biological perspectives: SEM, porosity measurement, FT-IR, XRD, and in-vitro degradation tests are used to characterize its structure, composition, and staged degradation; curcumin release is measured

2026 S.-T. Yau High School Science Award
仅用于2026丘成桐中学科学奖公示

under inflammatory pH 5.5 and physiological pH 7.4 conditions; LPS-stimulated RAW264.7 macrophages are used to evaluate M1/M2 polarization and IL-10 secretion; and MC3T3-E1 pre-osteoblasts are used to assess RUNX2 and ALP expression at both protein and mRNA levels. Through this integrated design, this study aims to demonstrate that the three-layer gradient scaffold can achieve tunable degradation, pH-responsive curcumin release, macrophage immunomodulation, and enhanced osteogenic induction, offering a promising biomaterial strategy for complex bone fracture repair.



Scheme 1. Schematic illustration of the design, fabrication, degradation, pH-responsive curcumin release, and biological functions of the curcumin-loaded three-layer gradient PLGA/HA scaffold

2 Materials and Methodology

2.1 Materials

2.1.1 Chemicals

PLGA with three different lactic-glycolic acid copolymer ratios (35:65, 50:50, 75:25) with a molecular weight of 40-60 kDa, Potassium bromide (KBr, spectral grade, CAS No. 7758-02-3), Concentrated hydrochloric acid (HCl, analytical grade, CAS 7647-01-0), Dichloromethane (DCM, 75-09-2), Lipopolysaccharide (LPS), and absolute ethanol were purchased from Adamas-beta (Shanghai, China). Nano-hydroxyapatite (HA, CAS: 1306-06-5, Cat. No.

2026 S.-T. Yau High School Science Award 仅用于2026丘成桐中学科学奖论文公示

H906378-25 g, purity ≥ 97%, particle size < 100 nm (BET)), Curcumin (CAS: 458-37-7, Cat. No. C138632, purity ≥ 98%, HPLC grade), Sodium chloride (NaCl, analytical grade), and Sterile phosphate-buffered saline (PBS, powder, pH 7.2-7.4) were obtained from Aladdin Biochemical Technology Co., Ltd. (Shanghai, China) Double-distilled water (ddH_2O) was self-prepared in the laboratory. Paraformaldehyde (PFA) fixative solution (Cat. No. G1101) was purchased from Wuhan Servicebio Technology Co., Ltd.

2.1.2 Cells and Reagents

MC3T3-E1 pre-osteoblast cells (CRL-2593) were obtained from ATCC. α-MEM (12571-063), DMEM, Fetal Bovine Serum (FBS), ALP primary antibody (PA5 106391), and RUNX2 Recombinant Rabbit Monoclonal Antibody (SD2080, MA5-41185) were obtained from Gibco. Penicillin-Streptomycin (P/S), Trypsin-EDTA solution (C0208-100ml), 5% Triton X-100 solution (P0096-100ml), confocal nuclear staining reagent (C1002), Mouse IL-10 high-sensitivity ELISA kit (Cat. No. PI521), RNAeasy™ Animal RNA Isolation Kit (R0024) were obtained from Beyotime Biotechnology (Shanghai, China). RAW264.7 macrophage cells were obtained from Cell Bank of Chinese Academy of Sciences. TB Green® Premix Ex Taq™ II (Tli RNaseH Plus; RR820A/B) and PrimeScript™ RT Master Mix (Perfect Real Time; RR036A) were obtained from Takara Biomedical Technology (Beijing) Co., Ltd.

2.1.3 Equipment

Scanning electron microscope (SEM, Regulus8230, Hitachi), Fourier transform infrared spectroscopy (FT-IR, Nicolet iS20, Thermo Fisher Scientific), X-ray diffraction (XRD, SmartLab SE, Rigaku), multi-mode microplate reader (CYTATION 3, BioTek), confocal laser scanning microscope (CLSM, FV3000, Olympus), CelMate CO_2 incubator (CLM-170B-8, Esco Lifesciences), Constant-temperature Shaker (MaxQ 420, Thermo Fisher Scientific), and laminar flow cabinet (SW-CJ-2FD, Hujing Purification) were used in this study.

2026 S.T. Yau High School Science Award
仅用于2026丘成桐中学科学奖论文公示

2.2 Experimental Methods

2.2.1 Fabrication of Scaffolds

The three-layer gradient scaffolds were fabricated by the solvent casting and salt leaching method [13]. Three precursor solutions with layer-specific PLGA/HA/curcumin compositions (**Table 1**) were prepared separately. Then, NaCl particles was added into each group as the agent to form pores.

Next, the three layers of the gradient scaffolds were sequentially cast. The inner-layer solution was first poured into a 10 cm-diameter Petri dish and oven-dried for 15 minutes for preliminary solidification. Then, the middle-layer precursor was cast on the pre-solidified inner layer and oven-dried for 15 minutes. Finally, the outer-layer solution was overlaid and cured to form an integrated three-layer scaffold (**Figure 1**).

Homogeneous single-layer curcumin-loaded scaffolds with 50:50 PLGA and HA/ curcumin amount same as the middle layer of the gradient scaffolds were fabricated to serve as the control group.



Figure 1. Process photos of scaffold synthesis with different PLGA/HA ratios and curcumin loading amounts

All scaffolds were fully dried before the removal of NaCl particles. NaCl particles were leached by continuous immersion in double-distilled water (ddH_2O). The leaching solution was replaced every 10 minutes for several repeated cycles to ensure complete removal of salt. After thorough leaching, all porous scaffolds were fully dried and stored in a dark, low-temperature environment for subsequent characterization and biological testing. All scaffold groups were prepared in multiple replicates for parallel experiments.

2026 S.-T. Yau High School Science Award 仅用于2026国际相关科学论文公示

Table 1. Formulation parameters for the outer, middle, and inner layers of three-layer gradient PLGA/HA/curcumin scaffolds prepared by solvent casting and salt leaching

Scaffold Layer Group (PLGA Ratio)	PLGA Mass	DCM Volume	HA Mass	Curcumin Dispersion Volume (60 mg/mL)	NaCl Mass
Outer layer (35:65)	1.2 g	15 mL	0.8 g	1.0 mL	2.0 g
Middle layer (50:50)	1.0 g	15 mL	1.0 g	0.83 mL	2.0 g
Inner layer (75:25)	0.6 g	15 mL	1.4 g	0.5 mL	2.0 g

2.2.2 Scaffold Material Characterization

SEM was used to observe the microscopic morphology and structural characteristics of the scaffolds. All fractured samples were sputter-coated with gold before imaging (**Figure 2**).



Figure 2. Process of sample preparation for SEM and microscopic morphology observation

Porosity was measured by the ethanol liquid displacement method. Dry weight (W_1) and wet weight (W_2) after immersion in absolute ethanol and vacuum degassing for 30 min were recorded. The scaffold was then submerged in ethanol (initial volume V_1; final volume V_2). The scaffold porosity was calculated according to the formula: $[(W_2 - W_1) / \rho_ethanol] / [(V_2 - V_1) + (W_2 - W_1) / \rho_ethanol] \times 100\%$, where $\rho_ethanol$ was set as 0.789 g/cm³. Five parallel samples (n=5) were tested for each group, and the average porosity was reported.

FT-IR and XRD were used to characterize the scaffolds. For FT-IR, dried, ground scaffold powder was mixed with spectroscopic-grade KBr and scanned from 4000 to 400 cm^{-1} at 4 cm^{-1}

2026 S.T.Yau High School Science Award
仅用于2026丘成桐中学科学奖论文公示

resolution with 32 scans. XRD was performed at 0 and 4 weeks to assess crystal structure changes, with 2θ scanned from 5° to 80°.

2.2.3 Degradation Performance

In-vitro degradation was assessed by dry weight loss. Initial dry mass was recorded, and scaffolds were immersed in pH 7.4 PBS in a constant-temperature shaker. At 1, 2, 3, and 4 weeks, samples were retrieved, dried, and weighed; the curve of remaining weight was plotted as the percentage of the initial weight.

2.2.4 pH-Responsive Curcumin Release Test

Curcumin-loaded three-layer gradient and homogeneous scaffolds were immersed in pH 7.4 or pH 5.5 PBS in 12-well plates, foil-wrapped to prevent photodegradation, and incubated in a constant-temperature shaker. After 0.5, 1, 2, 4, 6, 12, 24, 48, 72, 144, and 168 h, supernatants were collected, and absorbance was measured at 405 nm using a multimode microplate reader (**Figure 3**). Cumulative release was calculated from a pre-established curcumin standard curve generated by absorbance measurement of serially diluted curcumin solutions.

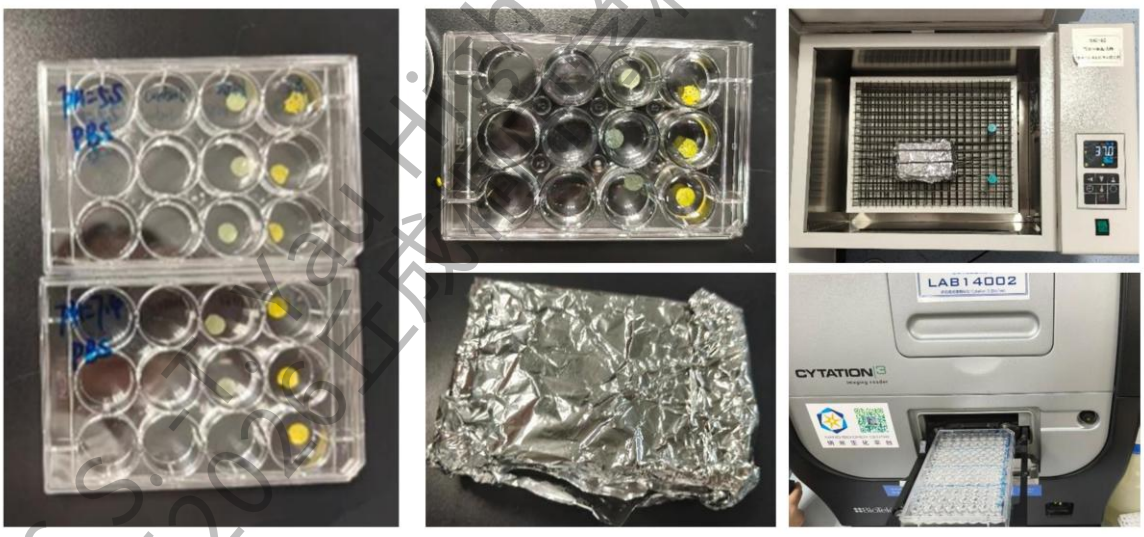


Figure 3. Photographs of the pH-responsive curcumin release experiment

2.2.5 Evaluation of Anti-inflammatory Effects

Macrophage Culture: RAW264.7 macrophages were cultured in high-glucose DMEM (10% FBS, 1% P/S) at 37 °C under 5% CO_2. Curcumin extract was prepared by incubating 100 mg gradient scaffold in 10 mL DMEM at 37 °C and 100 rpm for 24 h. The supernatant was

2026 Shanghai High School Science Award 仅用于2026上海市高中生科学奖论文公示

collected, centrifuged at 3000 rpm for 10 min and filtered through a 0.22 μm filter. Cells (2×10^5/well, 24-well) were treated for 24 h with three different medium groups and n=6 biological replicates: LPS (100 ng/mL), LPS (100 ng/mL) + free curcumin, or LPS (100 ng/mL) + curcumin extract; supernatants and cell pellets were collected.

Immunofluorescence Staining for Macrophage Polarization Assessment: RAW264.7 cells were harvested, PBS-washed, permeabilized, and incubated with antibody mixture (CD86-FITC/ iNOS-PE for M1; CD206-APC/Arg-1-PerCP for M2) at 4 °C in dark for 30 min. After PBS washing, samples were imaged by a confocal laser scanning microscope to analyze fluorescence intensity of M1 and M2 ((**Figure 4**).

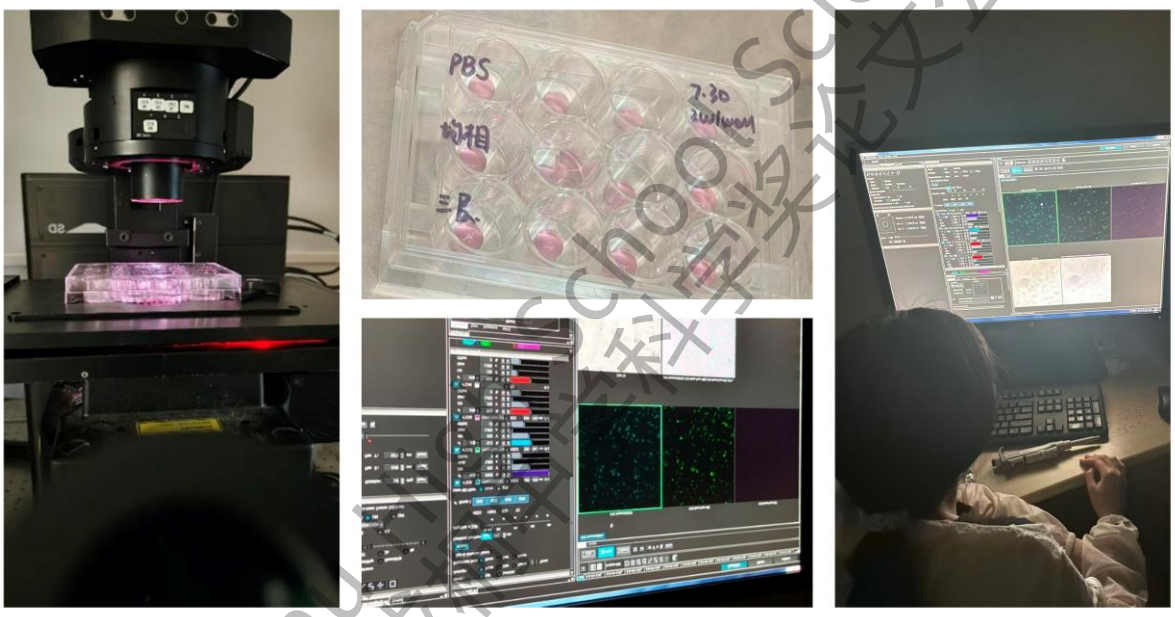


Figure 4. Workflow for immunofluorescence staining and imaging analysis of macrophage polarization

Detection of Inflammatory Factor (ELISA): The anti-inflammatory cytokine IL-10 in supernatants was quantified by ELISA using a mouse IL-10 standard curve constructed from serially diluted IL-10 standards (100-6.25 pg/mL). After samples were incubated, HRP-streptavidin and TMB were added; absorbance was measured at 450 nm after reaction was terminated, and IL-10 concentrations were calculated from the standard curve (**Figure 5**).

2026 S. T. Yau High School Science Award
仅用于2026丘成桐中学科学奖论文公示

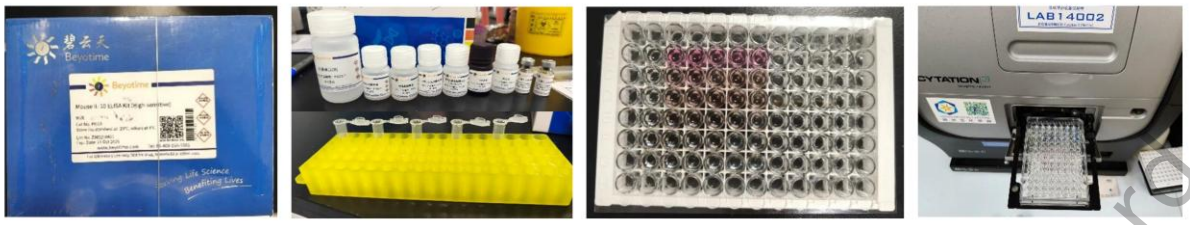


Figure 5. Experimental workflow for ELISA detection of the anti-inflammatory cytokine IL-10

2.2.6 Evaluation of Osteogenic Differentiation Performance

MC3T3-E1 Cell Culture and Seeding: In a laminar flow cabinet, MC3T3-E1 cells were thawed in a 37 °C water bath, centrifuged at 1000 rpm for 5 min, resuspended in α-MEM (10% FBS, 1% P/S), and cultured at 37 °C under 5% CO_2 for stable proliferation. Scaffolds were sterilized and pre-equilibrated with complete medium for 2 h, placed in a 24-well plate, seeded with cells suspension, and incubated statically for 4 h to allow cell attachment. Then, complete medium was added to each well and the samples were cultured at 37 °C (**Figure 6**).

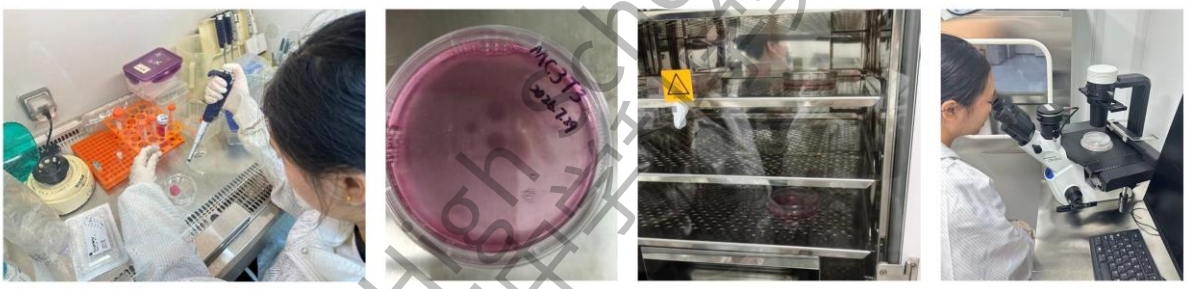


Figure 6. Resuscitation, subculture, and microscopic observation of MC3T3-E1 pre-osteoblasts in α-MEM complete medium

Immunofluorescence Staining of RUNX2 and ALP Osteogenic Proteins: At week 0, 2 and 4 after osteogenic induction, the scaffolds were removed and cells were fixed with PFA for 15 min at room temperature, permeabilized with 0.5% Triton X-100 for 15 min, and incubated with ALP or RUNX2 primary antibody at 37 °C for 1 h. After PBS rinses, the cells were incubated with secondary antibody overnight in a 4 °C refrigerator. Then nuclei were stained. After 10 min, samples were imaged by a confocal laser scanning microscope to analyze the fluorescence intensity and positive expression of the osteogenic proteins RUNX2 and ALP.

qPCR Analysis: At week 0, 2 and 4, cells were lysed and total RNA was isolated from cell lysates using RNAeasy™ Animal RNA Isolation Kit. The purified RNA was reverse-transcribed into complementary DNA using PrimeScript™ RT Master Mix. qPCR was

2026 S.T. Yau High School Science Award
仅用于2026丘成桐中学科学奖论文公示

conducted using TB Green® Premix Ex Taq™ II. RUNX2 and ALP gene expressions were normalized to GAPDH and calculated using the 2-ΔΔCt method.

3 Results and Discussion

3.1 Scaffold Morphology and Structure

Scanning electron microscope (SEM) was applied to characterize the fracture cross section and surface porous microstructure of the homogeneous and three-layer gradient scaffolds (**Figure 7**). The homogeneous scaffold exhibited a relatively smooth surface. Its surface featured small-sized pores that were densely packed and evenly distributed across the whole field of view, forming a uniform single-phase porous architecture. In comparison, the three-layer gradient scaffold displayed a visibly rougher surface. Distinct layered structures were clearly distinguished on its fracture surface. Its surface possessed larger and more irregular pores, which matched the design of three stacked layers with varied PLGA and HA blending ratios.

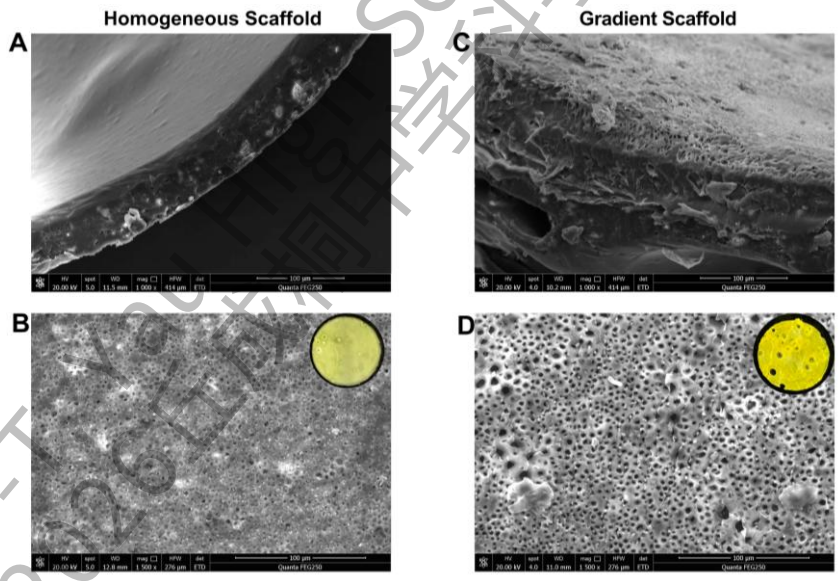


Figure 7. SEM morphological characterization of homogeneous scaffolds cross section(A) and surface (B), and three-layer gradient scaffolds cross section (C) and surface (D)

3.2 Porosity

Quantitative porosity measurement (**Figure 8**) revealed that the homogeneous scaffold had an average porosity of approximately 30 %. By contrast, the three-layer gradient scaffold achieved

2026 S.-T. Yau High School Science Award
仅用于2026丘成桐中学科学奖论文公示

around 65 % porosity, more than doubling the value of the homogeneous group. These numerical findings corroborate the qualitative observations from SEM, indicating that the three-layer gradient scaffold exhibited more open pore architecture.

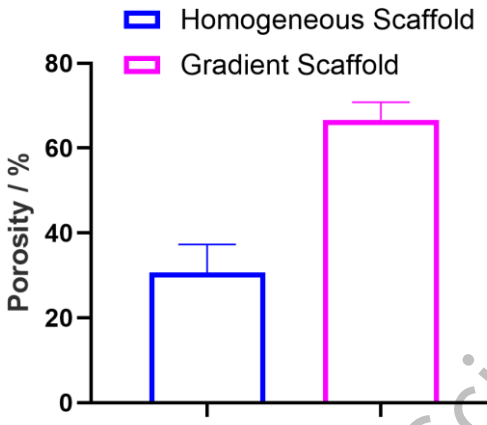


Figure 8. Porosity of homogeneous and three-layer gradient scaffolds

3.3 Chemical Structure (FT-IR Spectra)

Fourier transform-infrared spectroscopy (FT-IR) was used to assess chemical groups of the homogeneous and three-layer gradient scaffolds during 4-week in-vitro degradation. Peaks in the spectrum correspond to infrared absorption by specific chemical groups: PLGA-associated C=O stretching vibration peak near 1750 cm^{-1}, HA-associated P-O peak at 1000-1100 cm^{-1}, and O-H peak around 3300 cm^{-1}. A stronger absorption peak indicates higher relative content of the target groups [14].

Both types of scaffolds exhibited similar overall characteristic absorption peaks of PLGA and HA, confirming successful component compounding of the scaffolds (**Figure 9**). The C=O peak of the three-layer gradient scaffold became shallower at week 4, indicating the hydrolysis of PLGA. Meanwhile, a new minor absorption peak emerged beside the C=O peak near 1710 cm^{-1}, assigned to the hydrogen-bonded carboxylic acid (-COOH) groups generated by ester hydrolysis. The three-layer gradient scaffold also showed a broad O-H peak at week 4. This could be caused by hydroxyl-containing degradation by-products and absorbed moisture.

Despite that both scaffolds showed absorption peaks for similar chemical components, the shallower C=O peak, the newly emerged -COOH peak, and stronger O-H peaks at week 4 of the three-layer gradient scaffold indicated that the three-layer gradient scaffold underwent a

2026 Yau High School Science Award
仅用于2026年成相中学科学奖论文公示

faster degradation.

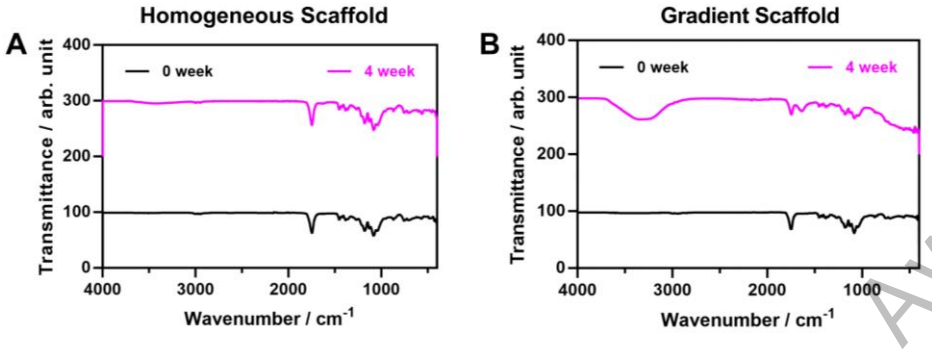


Figure 9. FT-IR spectroscopic characterization during in-vitro degradation of homogeneous and three-layer gradient scaffolds

3.4 Crystalline Structure

XRD was performed to characterize the crystal structure of the homogeneous scaffolds and three-layer gradient scaffolds. XRD curves from both groups (**Figure 10**) exhibited characteristic peaks dominated by PLGA at approximately 20° and HA-related diffraction peaks near 32° [15]. Compared with the homogeneous scaffold, the three-layer gradient scaffold displayed a broader PLGA diffraction peak, indicating a more distributed PLGA phase. This aligned with the varied PLGA ratios across the three distinct layers of the gradient scaffold. On the other hand, the three-layer gradient scaffold developed a much sharper HA diffraction peak. This sharp peak suggests a higher crystallinity or larger grain size of HA, which matched the designed gradient HA within the gradient scaffold. Collectively, these XRD results verified that the structural and compositional features of the two types of scaffolds were consistent with our material design, and further demonstrated that the three-layer gradient scaffold possessed a more complex crystallographic nature. At week 4, the homogeneous scaffold retained its main XRD features, with only slight changes in the PLGA halo at ~20° and the HA peaks at ~32°, consistent with its slower degradation. In contrast, the gradient scaffold showed a broader PLGA diffraction halo around 20°, indicating a more disordered PLGA phase after degradation. This can be attributed to the faster hydrolysis of PLGA in the gradient scaffold, which caused chain scission and reduced the amount of intact PLGA.

2026 Siyau High School Science Award 仅用于2026年度科学奖论文公示

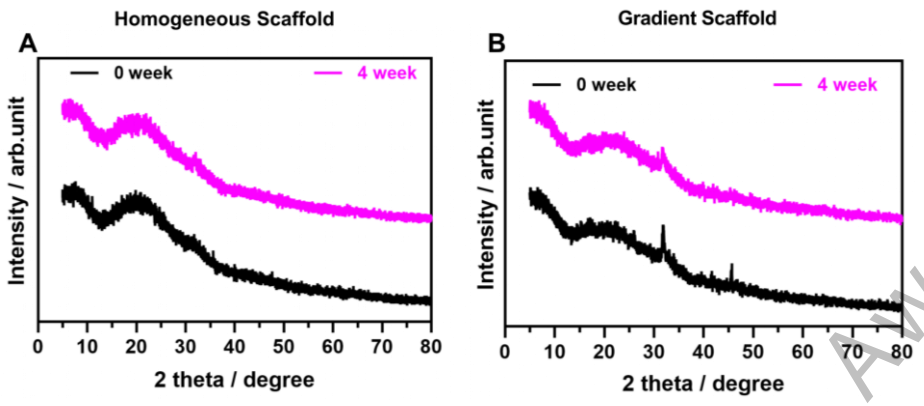


Figure 10. XRD profiles of the homogeneous and three-layer gradient scaffolds

3.5 Degradation Behavior

Macroscopic optical photographs were obtained for homogeneous and three-layer gradient scaffolds following 0, 2, and 4 weeks of in-vitro degradation. In addition, the remaining weight curves of both scaffolds were recorded over the 4-week in-vitro degradation period.

The optical images in **Figure 11A** showed progressive structural breakdown for both scaffold groups over the degradation period. From the remaining weight curve in **Figure 11B**, both scaffold groups exhibited continuous mass reduction throughout the 4-week test, indicating that degradation occurred in both scaffolds. At week 4, the three-layer gradient scaffold retained approximately 40% of its initial mass, whereas the homogeneous scaffold maintained around 60% of its original mass. This observation demonstrates that the three-layer gradient scaffold underwent faster degradation compared with the homogeneous scaffold. This outcome algins with our design rationale: the outer layer of the gradient scaffold with a 35:65 PLGA ratio will degrade faster than the homogeneous scaffold with a 50:50 PLGA ratio. The results verified that the degradation rate of PLGA-based scaffolds can be tuned by adjusting the PLGA monomer ratio.

Over the 4-week degradation period, the three-layer gradient scaffold exhibited rapid early-stage mass loss, which could open interconnected pore channels to facilitate cell migration, nutrient diffusion and new-tissue growth. This favorable early-stage rapid degradation is enabled by the layered architecture of the gradient scaffold: the outer layer degrades fast, while the inner layers are designed to degrade more slowly to preserve structural support for maturing newly-formed bone tissue. In contrast, the homogeneous scaffold adopts

2026 S. T. Yau High School Science Award
仅用于2026丘成桐中学科学奖论文公示

a uniform PLGA ratio throughout. To maintain long-term structural integrity, it must degrade at a slower overall rate, which consequently restricts its capacity to support cell migration and nutrient infiltration.

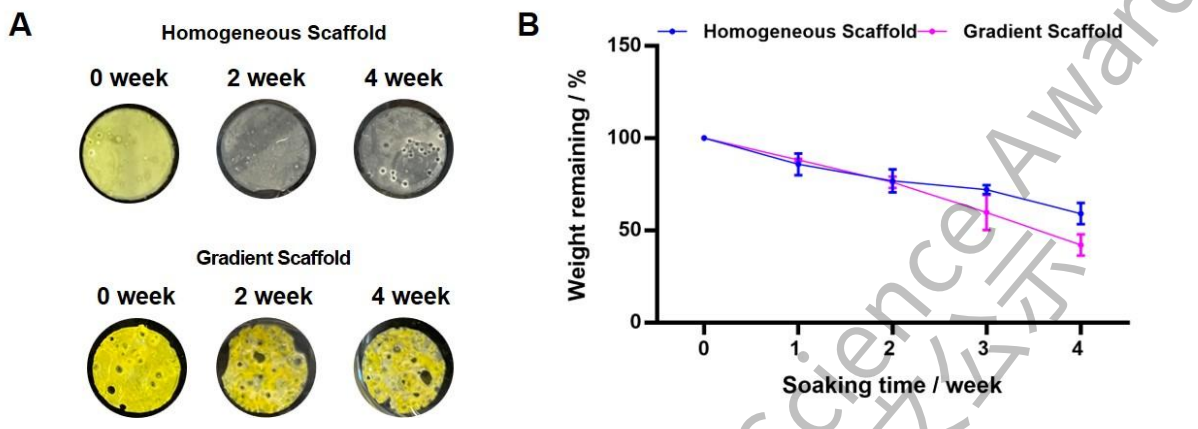


Figure 11. In-vitro degradation performance of homogeneous and three-layer gradient scaffolds

3.6 pH-responsive Drug Curcumin Profile

Curcumin release efficiency of homogeneous and three-layer gradient scaffolds was measured under pH 5.5 PBS simulating inflammatory bone microenvironment and pH 7.4 PBS simulating normal body microenvironment over 168 h using UV-Vis spectroscopy (**Figure 12**).

The three-layer gradient scaffold exhibited prominent pH-responsive curcumin release behavior. At acidic pH 5.5 PBS, the three-layer gradient scaffold achieved approximately 85-88% of cumulative curcumin release by 168 h, whereas under physiological neutral pH 7.4 PBS, drug release was substantially suppressed to around 50% at the same time point. In contract, the homogeneous scaffold showed much less pH-dependent responsiveness. Despite that it achieved a cumulative curcumin release rate comparable to that of the three-layer gradient scaffold under acidic conditions, its curcumin release rate reached approximately 63% at neutral pH by 168 h, substantially higher than that of the gradient scaffold. This pH-responsive release profile endows the three-layer gradient scaffold with a key advantage: drug release can be tailored to match the physiological microenvironment.

Curcumin release from scaffolds is jointly governed by molecular diffusion and PLGA matrix erosion. Acidic conditions accelerate PLGA degradation and theoretically promote drug release [16]. In this study, both scaffolds exhibited high total curcumin release at pH 5.5 PBS.

2026 S.T. Yau High School Science Award
仅用于2026丘成桐中学科学奖论文公示

The main group-specific distinction appeared under physiological pH 7.4 PBS, where the three-layer gradient scaffold effectively restrained drug release. This pH-responsive drug release behavior aligned with the material design intention: limiting premature drug leakage under healthy neutral tissue conditions while retaining sufficient curcumin payload for potential subsequent inflammatory episodes. The favorable drug release performance could be attributed to the stratified internal structure of the three-layer gradient scaffold which limited the occurrence of water penetration into the inner curcumin-loaded layers and thus hindered outward diffusion of embedded curcumin under normal physiological environment [17]. Such structure enabled the three-layer gradient scaffold to adapt to the dynamic microenvironment during bone repair and supported sustained targeted therapeutic function. Its ability to limit therapeutic drug release under healthy tissue microenvironments could also prevent potential cytotoxic effects as high concentrations of bioactive agents can impair normal cell viability in non-inflamed tissue [18]. As such, compared with the homogeneous scaffold, the three-layer gradient scaffold possesses remarkable advantages of pH-responsive drug release behavior and sustained drug release for bone regeneration.

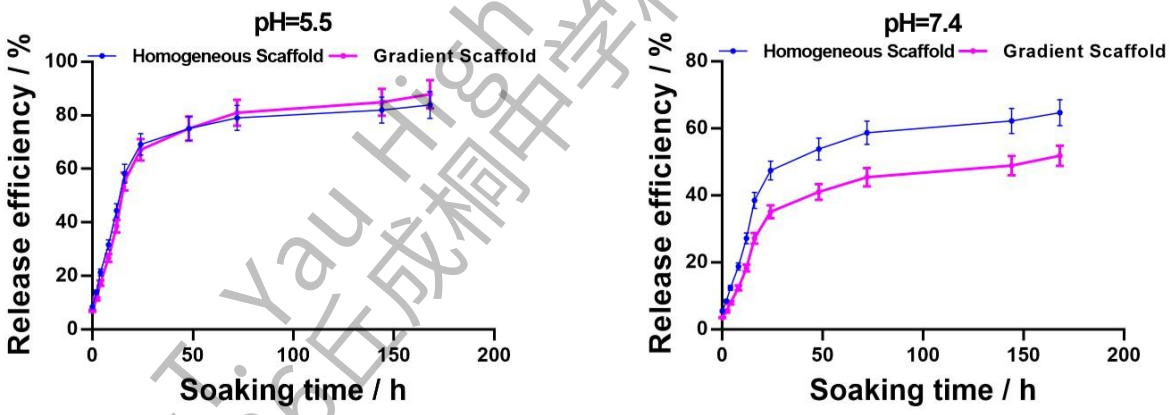


Figure 12. Curcumin release behavior under different pH conditions for homogeneous and three-layer gradient scaffolds

3.7 Anti-inflammatory Effect

Immunofluorescence staining was used to evaluate M1 macrophage polarization of three different experiment groups. Confocal laser scanning microscope was used to observe and analyze the fluorescence intensity of M1 (**Figure 13**).

2026 S.T. Yau High School Science Award
仅用于2026丘成桐中学科学奖论文公示

The LPS group, RAW264.7 cells cultured in medium with only LPS, showed strong fluorescence, indicating obvious pro-inflammatory M1 polarization. The free curcumin group (RAW264.7 cells cultured in medium with LPS and free curcumin) and the gradient scaffold group (RAW264.7 cells cultured in medium with LPS and curcumin released from the three-layer gradient scaffold) both showed significantly reduced intensity of fluorescence. This proved that curcumin successfully inhibited LPS-induced M1 inflammatory responses. On the other hand, the gradient scaffold group showed similar anti-inflammatory effects compared with free curcumin group, which indicated that the curcumin released from the scaffold remained biologically functional and could effectively suppress pro-inflammatory macrophage polarization [19].

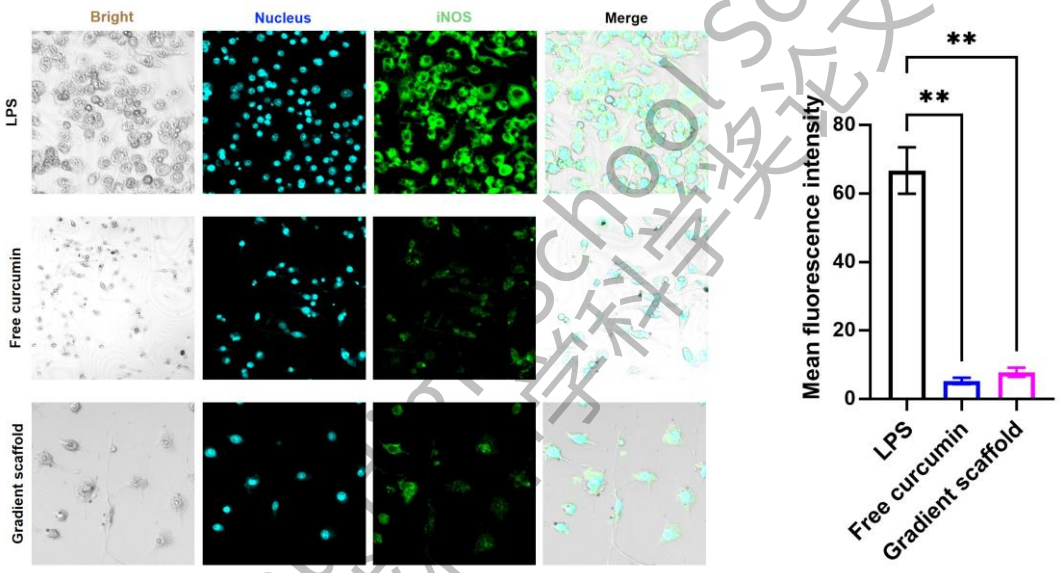


Figure 13. Immunofluorescence analysis of M1 macrophage polarization

Immunofluorescence staining was used to evaluate anti-inflammatory M2 macrophage polarization with CD206 as a specific M2 marker. The LPS group showed very low CD206 expression, as observed both from the immunofluorescence images and the quantitative fluorescence intensity bar graph. The free curcumin group exhibited only a slight increase in CD206 intensity, with no significant difference from the LPS group. In contrast, the gradient scaffold group presented a remarkably higher CD206 signal, showing strong M2 polarization. The prominent M2 polarization is favorable for alleviating inflammation and creating a supportive microenvironment for bone healing (**Figure 14A**).

To further verify the M2-polarizing effect, ELISA was applied to detect the secretion of

2026 S.-T. Yau High School Science Award
仅用于2026丘成桐中学科学奖公示

IL-10, a key anti-inflammatory cytokine mainly secreted by M2-typed macrophages. As shown in **Figure 14B**, the gradient scaffold group produced markedly higher IL-10 levels compared with the LPS group and the free curcumin group. These ELISA findings corroborated the immunofluorescence results, demonstrating that the three-layer curcumin-loaded gradient scaffold effectively drove macrophages towards the anti-inflammatory M2 phenotype and elevate secretion of IL-10, and thus possessed a strong advantage of reducing inflammation, supporting tissue repair and promoting bone regeneration. [20]

Interestingly, unlike the gradient scaffold, free curcumin failed to induce obvious M2 polarization under the current experimental conditions, which was an unexpected finding. One possible explanation for this phenomenon is that the curcumin extract from the gradient scaffold was collected after 24 h of scaffold soaking. During incubation, HA within the scaffold may have partially dissolved and released calcium and phosphate ions into the medium. These ions have been reported to activate the calcium-sensing receptor (CaSR) and downstream Wnt/β-catenin signaling in macrophages, which could in turn contribute to M2-type anti-inflammatory polarization. Therefore, the M2-polarizing effect of the gradient scaffold extract may not be solely attributable to curcumin and could also involve HA-derived ionic cues [21]. However, this remains speculative because Ca/P release, CaSR activation, and Wnt/β-catenin signaling were not directly measured in this study. Further experiments using HA-free scaffolds, curcumin-free gradient scaffolds, and CaSR/Wnt inhibitors are needed to verify this possibility.

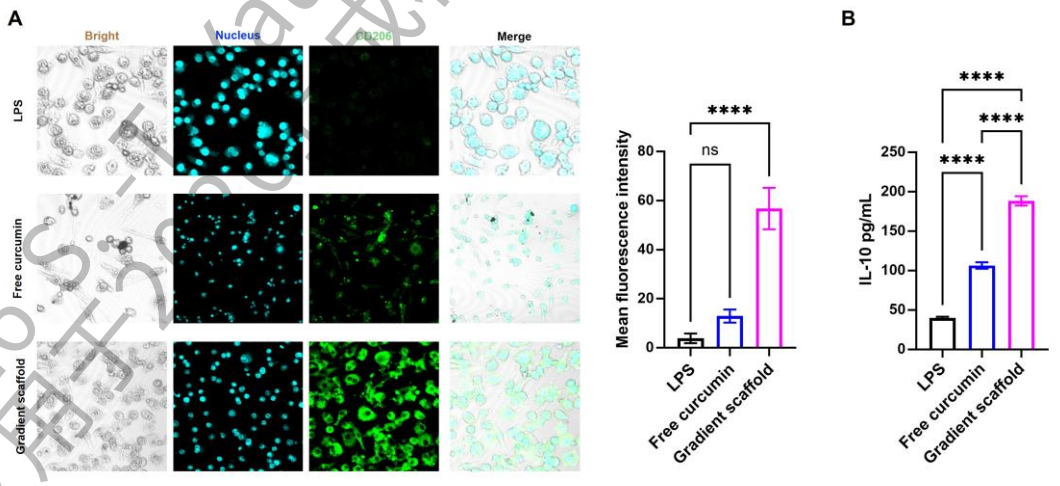


Figure 14. Immunofluorescence analysis of M2 macrophage polarization (A) and ELISA analysis of IL-10 secretion (B)

2026 S-Hua High School Science Award
仅用于2026年华为高中科学奖公示

3.8 Osteogenic Differentiation

The immunofluorescence assay targets two key osteogenic proteins: RUNX2, an early osteogenic marker [22] and ALP, a mid-stage osteogenic marker [23]. Immunofluorescence staining was performed for homogeneous and three-layer gradient scaffold groups at week 0, 2 and 4. RUNX2 was labelled with green fluorescence, ALP was labelled in magenta, and cell nuclei were stained blue. Higher fluorescence intensity corresponds to stronger expression of these osteogenic proteins (**Figure 15**).

At week 0, both scaffold groups displayed similar cell density and nearly undetectable RUNX2 and ALP fluorescence signals, confirming identical starting conditions for cell differentiation. As culture proceeded, fluorescence brightness for both RUNX2 and ALP increased in both groups. Notably, the three-layer gradient scaffold exhibited stronger and denser green RUNX2 and magenta ALP signals compared with the homogeneous group at week 2 and week 4. Cells cultured with three-layer gradient scaffolds also showed more spread-out morphology.

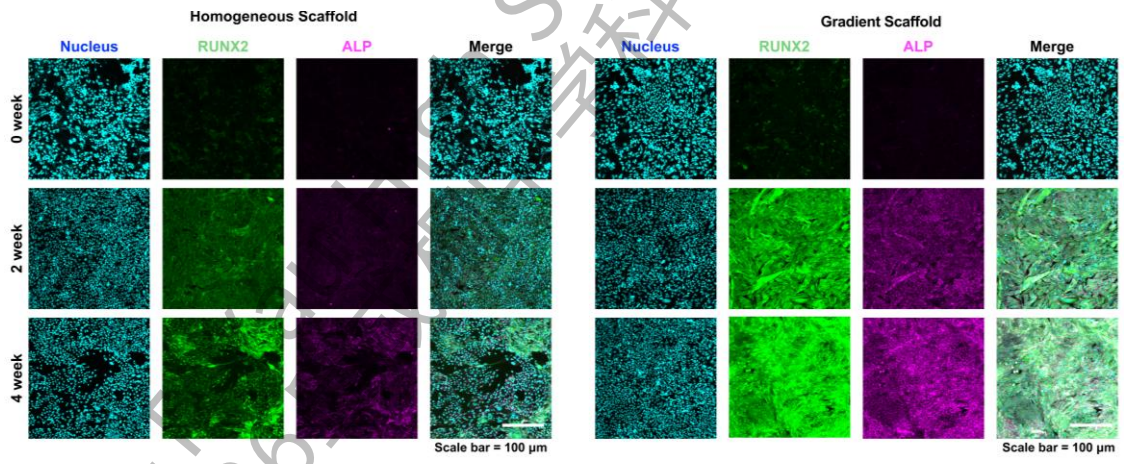


Figure 15. Immunofluorescence analysis of osteogenic markers for homogeneous and three-layer gradient scaffolds

Quantitative analysis of immunofluorescence was conducted to compare fluorescence intensity of RUNX2 and ALP on homogeneous and three-layer gradient scaffold groups. At week 0, no significant difference was detected for either marker between the two groups. The mean fluorescence intensity of RUNX2 and ALP increased over time in both scaffold groups. At week 2 and week 4, the three-layer gradient scaffold showed significantly higher RUNX2

2026 S-[illegible] School Science Award
仅用于2026[illegible]科学论文大赛

intensity (**** $p < 0.0001$) compared with the homogeneous scaffold. Similarly, significant differences of ALP intensity appeared at week 2 (** $p < 0.01$) and became more pronounced at week 4 (**** $p < 0.0001$) (**Figure 16**). These quantitative results matched the visual observation from immunofluorescence images.

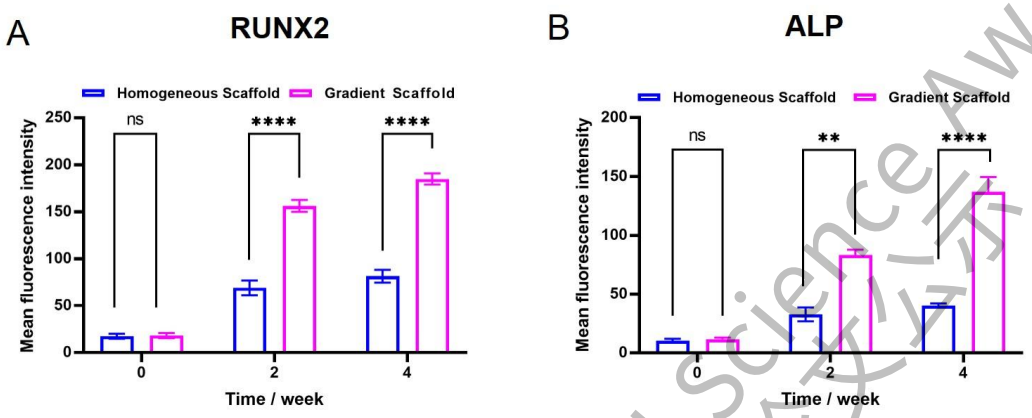


Figure 16. Quantitative fluorescence intensity of osteogenic markers for homogeneous and three-layer gradient scaffolds

In addition, qPCR was performed to quantify the fold change of RUNX2 mRNA and ALP mRNA on homogeneous and three-layer gradient scaffold groups (**Figure 17**). At week 0, RUNX2 mRNA and ALP mRNA levels were comparable between the two groups, confirming same initial gene expression status. RUNX2 mRNA and ALP mRNA levels increased over time in both groups. At week 2 and week 4, the three-layer gradient scaffold group displayed significantly higher RUNX2 mRNA and ALP mRNA fold change compared with the homogeneous group (**** $p < 0.0001$).

Since both scaffolds were cultured under identical initial cell conditions, the enhanced osteogenic protein expression of the three-layer gradient scaffold, evidenced by immunofluorescence staining images, quantitative analysis of fluorescence intensity, and qPCR transcriptional data, provides support for its superior osteogenic differentiation capacity. This strong osteogenic performance can be attributed to its porous and layered architecture, which creates a better porous microenvironment to facilitate cell infiltration into the scaffold, efficient nutrient transport, and subsequent new-tissue ingrowth [24], and thus provides physical cues that effectively promote osteogenic differentiation of seeded cells.

2026 S.-T. Yau High School Science Award
仅用于2026丘成桐中学科学奖论文公示

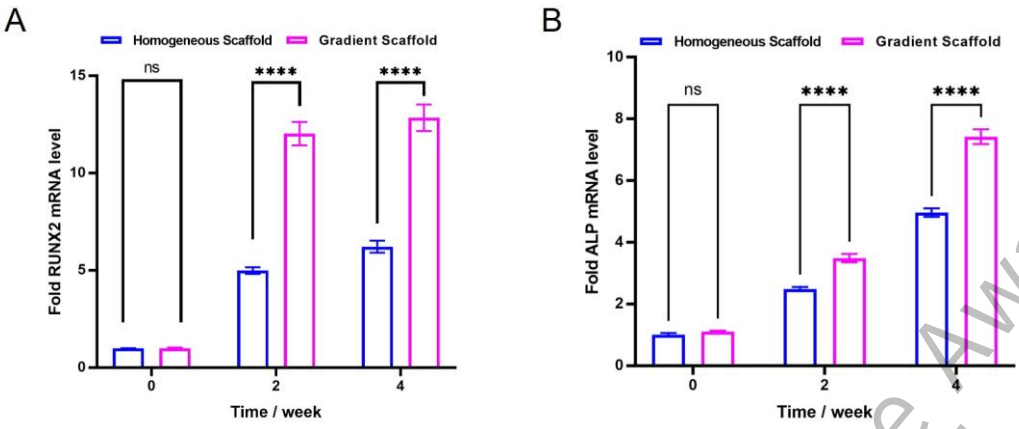


Figure 17. qPCR gene expression analysis of osteogenic markers for homogeneous and three-layer gradient scaffolds

4 Future Plan

Future work will address three limitations. First, since the three-layer gradient scaffold group outperformed the free curcumin group in M2 polarization, HA-derived chemical cues and structural cues may also contribute; direct cell seeding on the gradient scaffold with curcumin-free/HA-free controls will be implemented to decouple these effects [25]. Second, degradation monitoring will be extended from 4 to 12 weeks to match the full timeframe for typical bone healing and optimize PLGA ratios. Third, in vivo implantation in animal models will be performed to validate the three-layer gradient scaffold's performance under physiological microenvironments and the host immune system to provide more robust evidence and move our findings closer to clinical application for bone-defect treatment.

5 Conclusion

In conclusion, this study developed a curcumin-loaded three-layer gradient PLGA/HA scaffold that outperformed homogeneous scaffolds for complex bone repair, as its layered porous structure and tunable PLGA/HA ratios enabled favorable cell infiltration and staged degradation, and significantly enhanced the expression of osteogenic markers RUNX2 and ALP at both protein and mRNA levels; it also exhibited pH-responsive curcumin release, reducing premature leakage at pH 7.4 while allowing sufficient release under inflammatory pH 5.5, and effectively suppressed M1 polarization, promoted M2 polarization, and increased IL-

2026 Yau High School Science Award 仅用于2026亚成利中学科学奖论文公示

10 secretion for anti-inflammatory regulation. This scaffold integrates staged degradation, immunomodulation, and osteogenic induction, and represents a promising candidate for complex bone fracture repair that warrants further in vivo validation.

2026 S.-T. Yau High School Science Award
仅用于2026丘成桐中学科学奖论文公示

References

[1] GBD 2019 Fracture Collaborators. Global, regional, and national burden of bone fractures in 204 countries and territories, 1990–2019: a systematic analysis from the Global Burden of Disease Study 2019[J]. The Lancet Healthy Longevity, 2021, 2(9): e580-e592.

[2] Zura R, Xiong Z, Einhorn T, et al. Epidemiology of fracture nonunion in 18 human bones[J]. JAMA Surgery, 2016, 151(11): e162775.

[3] Khodaei T, Schmitzer E, Suresh A P, et al. Immune response differences in degradable and non-degradable alloy implants[J]. Bioactive Materials, 2023, 24: 153-170.

[4] Nair L S, Laurencin C T. Biodegradable polymers as biomaterials[J]. Progress in Polymer Science, 2007, 32(8-9): 762-798.

[5] Sultana N. Biodegradable Polymer-Based Scaffolds for Bone Tissue Engineering[M]. Berlin: Springer Nature, 2013.

[6] Zhu G, Zhang T, Chen M, et al. Bone physiological microenvironment and healing mechanism: Basis for future bone-tissue engineering scaffolds[J]. Bioactive Materials, 2021, 6(11): 4110-4140.

[7] Polo-Corrales L, Latorre-Esteves M, Ramirez-Vick J E. Scaffold design for bone regeneration[J]. Journal of Nanoscience and Nanotechnology, 2014, 14(1): 15-56.

[8] Zadpoor A A. Bone tissue regeneration: the role of scaffold geometry[J]. Biomaterials Science, 2015, 3(2): 231-245.

[9] Wang Z, Cao W, Wu F, et al. A triphasic biomimetic BMSC-loaded scaffold for osteochondral integrated regeneration in rabbits and pigs[J]. Biomaterials Science, 2023, 11(8): 2924-2934.

[10] Makadia H K, Siegel S J. Poly lactic-co-glycolic acid (PLGA) as biodegradable controlled drug delivery carrier[J]. Polymers, 2011, 3(3): 1377-1397.

[11] Dorozhkin S V. Bioceramics of calcium orthophosphates[J]. Biomaterials, 2010, 31(7): 1465-1485.

[12] D’Angelo F N A, Paulo J, Lopes A M, et al. Selection and Control of Process Conditions Enable the Preparation of Curcumin-Loaded Poly(lactic-co-glycolic acid) Nanoparticles of Superior Performance[J]. ACS Applied Materials & Interfaces, 2023, 15(22): 26496-26509.

2026 Siyau High School Science Award 仅用于2026年成都中学科学奖论文公示

[13] Adel I M, ElMeligy M F, Elkasabgy N A. Conventional and Recent Trends of Scaffolds Fabrication: A Superior Mode for Tissue Engineering[J]. Pharmaceutics, 2022, 14(2): 306.

[14] Higuchi J, Fortunato G, Woźniak B, et al. Polymer Membranes Sonocoated and Electrosprayed with Nano-Hydroxyapatite for Periodontal Tissues Regeneration[J]. Nanomaterials, 2019, 9(11): 1625.

[15] Šupová M, et al. Multifunctional hydroxyapatite and poly (D, L-lactide-co-glycolide) nanoparticles for the local delivery of cholecalciferol[J]. Journal of Nanobiotechnology, 2014, 12(1): 48.

[16] Zolnik B S, Burgess D J. Effect of acidic pH on PLGA microsphere degradation and release[J]. Journal of Controlled Release, 2007, 122(3): 338-344.

[17] Xu Q, Chin S E, Wang C H, et al. Mechanism of drug release from double-walled PDLLA(PLGA) microspheres[J]. Biomaterials, 2013, 34(15): 3902-3911.

[18] Bhattacharjee A, Jo Y, Bose S. In vivo and In vitro properties evaluation of curcumin loaded MgO doped 3D printed TCP scaffolds[J]. Journal of Materials Chemistry B, 2023, 11(21): 4725-4739.

[19] Guo P, Ibrahim M A A, Zhang H, et al. Curcumin mediates macrophage polarization to inhibit the formation of abdominal aortic aneurysms by inhibiting the expression of histone acetyltransferase EP300[J]. Arabian Journal of Chemistry, 2023, 16(11): 105227.

[20] Rőszer T. Understanding the mysterious M2 Macrophage through activation markers and effector mechanisms[J]. Mediators of Inflammation, 2015, 2015: 816460.

[21] Xiao L, Shiwaku Y, Hamai R, et al. Macrophage polarization related to crystal phases of calcium phosphate biomaterials[J]. International Journal of Molecular Sciences, 2021, 22(21): 11252.

[22] Bruderer M, Richards R G, Alini M, et al. Role and regulation of RUNX2 in osteogenesis[J]. European Cells and Materials, 2014, 28: 269-286.

[23] Huang W, Yang S, Shao J, et al. Signaling and transcriptional regulation in osteoblast commitment and differentiation[J]. Frontiers in Cell and Developmental Biology, 2021, 9: 689728.

[24] Murphy C M, O’Brien F J. Cell-scaffold interactions: the effect of pore size and porosity on cellular behaviour[J]. Cell Adhesion & Migration, 2010, 4(3): 377-381.

2026 S.-T. Yau High School Science Award
仅用于2026丘成桐中学科学奖公示

[25] Yang T, Fang Z, Zhang J, et al. Physical cues in biomaterials modulate macrophage polarization for bone regeneration: a review[J]. Frontiers in Bioengineering and Biotechnology, 2025, 13: 1640560.

2026 S.-T. Yau High School Science Award
仅用于2026丘成桐中学科学奖论文公示

Acknowledgements

I would like to express my deepest gratitude to all those who have offered me support, guidance, and assistance throughout this study.

This project originated from my personal experience of a toe fracture, followed by internal fixation with steel implants and subsequent implant-removal surgery. This painful experience sparked my strong interest in research on degradable biomaterials for bone repair.

Upon advancing to high school, I shared my research interest with Mr. Liao from the school's STEM Office. He was the person who helped me the most in this study. He encouraged me to read research papers about biodegradable composite scaffolds for bone regeneration. He gave me valuable ideas about how to conduct literature review and how to narrow down to my core research question. He guided me in theoretical learning, introduced me to data analysis methods, and provided insightful comments on my research plan. His expertise in biology and chemistry enabled him to provide ample support whenever I faced technical challenges in this study. He engaged me in in-depth academic discussions and actively cultivated my critical thinking. In addition, he gave me valuable suggestions for my paper writing. I sincerely thank him for his selfless and continuous encouragement, guidance, and support throughout the entire journey of this study, which greatly improved my academic literacy and research capabilities.

I would also like to extend my gratitude to Mr. Gao for granting me free access to the biomaterials research laboratory facilities and necessary experimental materials. He gave me valuable guidance about laboratory safety, operations of various experimental equipment, preparation of chemical reagents, and as well as data analysis. Throughout the experiment process, his technical support and advice helped me to plan and conduct my experiments efficiently. He also provided me with practical suggestions when I ran into experimental obstacles. For example, I encountered a major challenge: the universal material testing machine was not feasible for evaluating the scaffold degradation because of the limited dimensions of my prepared scaffold specimens. He offered me with multiple alternative approaches. Inspired by his inputs, I combined qualitative observation of scaffold morphology with quantitative mass-loss measurement to assess scaffold degradation in my experiments.

Furthermore, I would like to acknowledge the foundational work of the numerous

2026 Tiyau High School Science Award
仅用于2026年成利中学科学奖论文公示

researchers cited in this paper. Their pioneering studies provided the essential context and motivation for my project. I also wish to thank my homeroom teacher, who is also my chemistry teacher. Through his classes and the chemistry club he leads, I acquired extensive chemistry knowledge that laid a solid academic foundation for this study.

Finally, I would like to acknowledge Doubao, an AI tool, for its assistance in helping me to polish academic language. I used this tool intermittently over several months for language revision and manuscript refinement during project writing.

Throughout this research journey, I expanded my knowledge in biomaterials, gained hands-on experience in research and investigation, enhanced my experimental skills, and improved my critical thinking and problem-solving capacities. I am truly grateful to everyone who gave me support, guidance, assistance and encouragement along the way. And all guidance for this project was provided voluntarily without compensation.

2026 S.-T. Yau High School Science Award
仅用于2026丘成桐中学科学奖论文公示